LANGMUIR

Article

pubs.acs.org/Langmuir

Vapor-Phase Carbenylation of Hard and Soft Material Interfaces

Xunzhi Li, Wenchuan Ma, and Alexander A. Shestopalov*

Department of Chemical Engineering, University of Rochester, Rochester, New York 14627, United States

Supporting Information

ABSTRACT: This study describes the formation of functional organic monolayers on hard and soft interfaces via a vapor-phase carbene insertion into Si−H and C−H bonds. We demonstrate that functional diazirine molecules can be used to form monomolecular coatings on silicon, silicon nitride, and urethane−acrylate polymers under mild vacuum conditions and exposure to UV light. We investigate the molecular coverage and the long-term stability of the resulting monolayers in air, isopropanol, and water. Our results suggest that vapor-phase carbenylation can be used as a complementary technology to the traditional self-assembly, permitting functionalization of various passivated substrates with stable and functional molecular coatings under mild and scalable conditions.

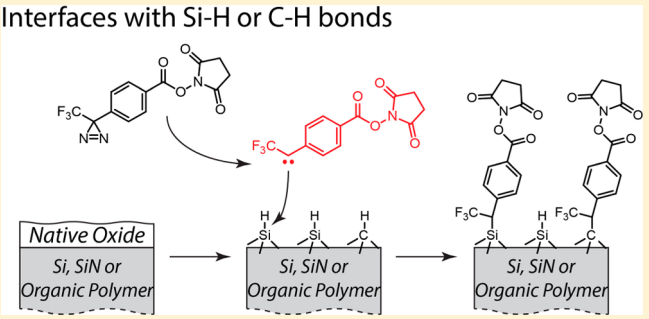

INTRODUCTION

A control over the interfacial properties with a single monomolecular layer is desired for the next generation of ultracompact, functional coatings. Such technology would catalyze implementation of multiple innovations in heterogeneous catalysis,[1] material selection, separation and filtration,[2] interfacial adhesion and friction,[3,4] and thin-film electronic devices.[5−7]

Formation of chemisorbed organic monolayers relies on the chemical reaction between an activated surface and functional organic molecules. To form a stable monolayer, this reaction should functionalize all reactive surface sites and form thermodynamically stable, nonhydrolytic surface bonds. Because it is difficult to achieve simultaneous complete surface coverage and stable attachment, another approach is often used instead: the molecules are selected to have symmetrical structures that can form ordered two-dimensional phases stabilized by the extensive van der Waals (VdW) interactions. Such self-assembled monolayers (SAMs) can shield unreacted surface sites from the environment or provide additional stabilization energy to the monolayers that rely on semicovalent or hydrolytic surface bonds. The SAM approach, initially discovered by Nuzzo and Allara in the early 1980s,[8] has been demonstrated on all major classes of inorganic materials and was utilized in many branches of science as a simple and powerful way to control physical, chemical, and biological properties of inorganic materials.[9−11] However, the same feature that brings additional stability to the monolayer and shields the interface from the environment—the ability of centrosymmetric molecules to form ordered, two-dimension aggregates—somewhat restricts the variety of molecules and surfaces that can form and support stable and functional SAMs. Typically, the SAM approach encounters challenges with functionalization of (1) rough interfaces where the surface defects preclude molecular self-assembly[12−17] and (2) soft materials and polymers due to their decreased stability and chemical inertness or low density of the reactive surface sites. SAMs also have limitations associated with the diversity of molecules that can participate in the self-assembly: (3) monolayers bearing large terminal functional groups are generally much less stable due to the relatively low order in the organic phase,[11,18−20] whereas formation of uniformly mixed SAMs with functional and inert components is also limited because of their phase segregation into distinctive monocomponent domains.[21−23]

The alternative strategy, which avoids some of the SAM limitations, relies on the attachment of functional organic molecules to passivated surfaces via stable nonpolar bonds. This approach has been successfully demonstrated in functionalization of different forms of carbon and silicon.[24−29] Stable H-terminated silicon, diamond, carbon nanotube, and graphene sheets can be reacted with organic alkenes and alkynes to form highly stable monolayers that are connected to the surfaces through Si−CH_X and C−CH_X bonds. These monolayers demonstrate high hydrolytic and thermal stability. However, the formation of such monolayers relies on harsh liquid-phase hydroalkylation and hydrosilylation reactions that typically require chemical catalysts, specific solvents, or high temperatures—conditions incompatible with many inorganic films, organic functional groups, and polymers. Another alternative strategy is the carbene insertion into the surface Si−H and C−H bonds (Figure 1).[29−31] We have previously demonstrated that solution-phase reactions of functional carbene precursors can be used to modify simple Me-terminated SAMs on silicon,

Received: July 4, 2016
Revised: October 19, 2016
Published: October 19, 2016

DOI: 10.1021/acs.langmuir.6b02471
Langmuir XXXX, XXX, XXX−XXX

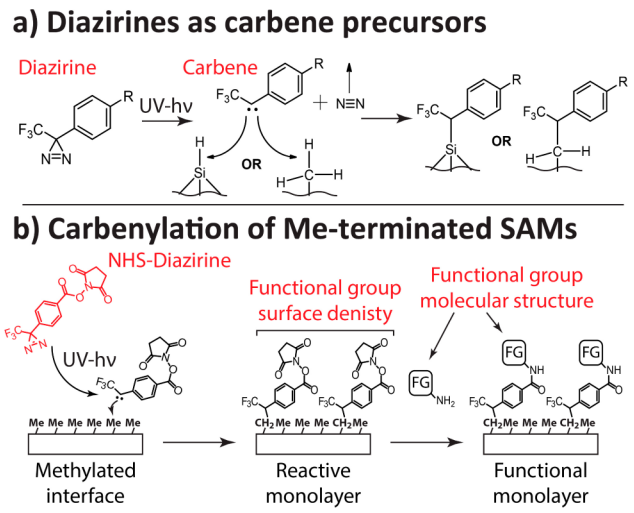

Figure 1. (a) Generation of reactive carbenes from diazirines and carbene insertion into Si−H and CH_2−H bonds; (b) formation of reactive and functional monomolecular coatings on methylated interfaces.

silicon oxide, germanium, and indium tin oxide.[7,32−35] We showed that the carbene reactions on these methylated surfaces produce largely identical functional monolayers. However, a limitation to our methodology was the solution-phase processing in inert carbon tetrachloride, which significantly limits the throughput and substrate area, requires extensive substrate cleaning, and makes the functionalization incompatible with the majority of soft and nanostructured materials due to the swelling and capillary effects.

In this study, we report a functionalization approach that utilizes mild vapor-phase conditions to form stable and functional monolayers on passivated inorganic and organic interfaces. Our approach relies on a vapor-phase carbenylation reaction that creates stable and nonhydrolytic Si−C and C−C bonds between the molecules and the substrates. Our method utilizes diazirines as functional carbene precursors (Figure 1). Diazirines are well-known photolabeling reagents and heterobifunctional linkers that generate reactive carbenes in 365 nm UV light.[36−48] The generated carbenes can selectively react with $-CH_3$ groups and participate in the insertion into the interfacial Si−H and C−H bonds.[7,29,31−35] Various diazirines can be synthesized with reactive moieties that do not participate in the self-propagating carbene insertion (e.g., *N*-hydroxysuccinimide (NHS) esters, amide and ester groups, aromatic rings, and C−Hal bonds) but can be easily converted into other functionalities following the carbenylation. We demonstrate that this method avoids the limitations of the solution-phase reactions and permits direct functionalization of inorganic and organic materials with stable and functional molecular coatings.

MATERIALS AND METHODS

Materials. We used 2,5-dioxopyrrolidin-1-yl 4-(3-(trifluoromethyl)-3*H*-diazirin-3-yl)benzoate (**NHS-diazirine**) as a carbene precursor. This molecule releases diatomic nitrogen and generates reactive carbene species when exposed to UV light. The generated carbenes readily react with the surface Si−H and C−H bonds; however, they do not participate in the self-condensation reactions, limiting their films to single monolayers.[29−31] **NHS-diazirine** was synthesized in 10 steps following the previously published protocol (Figure 1S shows the reaction scheme and detailed experimental details).[35,49,50] The calculated bulk density of the solid **NHS-diazirine** is 1.68 g/cm^3 (calculated using Advanced Chemistry Development (ACD/Laboratories) software, version 11.02). The bulk density of **NHS-diazirine** was used to calculate the inelastic mean free path (the attenuation length) of the photoelectrons in the **NHS-diazirine** film. To estimate the thickness of a single **NHS-diazirine** monolayer, we replaced the diazirine cycle in the **NHS-diazirine** 3D model with the CH−SiH_3 bond and aligned its direction with the surface normal. After minimizing the molecular energy, the calculated height of the model molecule was 10.75 Å (calculated using PerkinElmer Chem3D software, version 15.1, Figure 2S).

We used polycrystalline silicon (**Si**: <1−1−1> prime wafer, N type, As doped), thermally grown silicon nitride (**SiN**: 400 nm film on Si <1−0−0> prime wafer, N type, Ph doped), and a polyurethane−acrylate polymer (**PUA**, Figures 2 and 3S) as the substrates for the

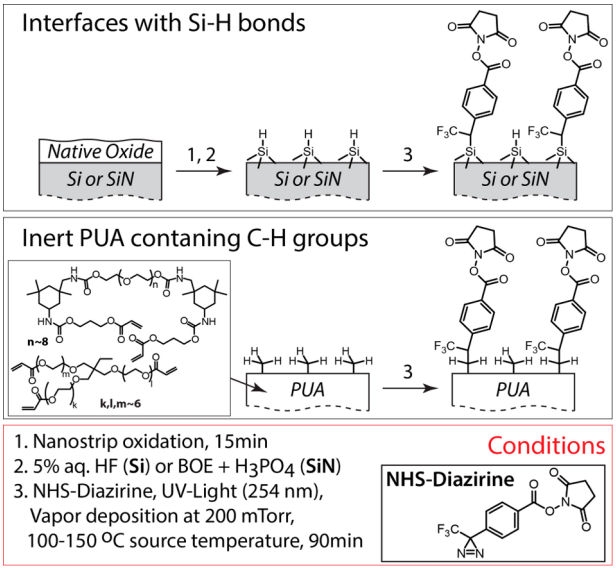

Figure 2. Formation of NHS-terminated monolayers on **Si**, **SiN**, and **PUA**. Chemical composition of the **PUA** polymer and reactive conditions.

carbene-insertion reactions. **Si** and **SiN** were passivated prior to the carbene insertion to remove the native oxide layer and to terminate surface-exposed Si atoms with hydrogens (see Supporting Information for the detailed protocols and conditions). X-ray photoelectron spectroscopy (XPS) was conducted on the passivated **SiN** to determine its molecular composition ($Si_{38.76}$, $N_{50.20}$, $O_{11.04}$). **PUA** composition was calculated from its chemical formula ($C_{69.72}H_{28.36}N_4O_{7.4}$). The **Si** substrate was assumed to be pure silicon. These substrates were selected to examine how the coverage of the **NHS-diazirine** monolayers changes on interfaces with high and low concentrations of the surface-reactive sites (Si−H bonds on **Si** and **SiN** vs surface C−H bonds on **PUA**) and how the stability of the carbene monolayers is affected by the substrate tendency to form native oxide layers.

Experimental Section. The vapor-phase deposition of **NHS-diazirine** was conducted in a glass vacuum chamber at 200 mTorr of pressure. The substrate was positioned 10 cm away from the source containing 7.5 mg of **NHS-diazirine**. The source was heated to melt the **NHS-diazirine** (~130 °C), and the UV light was introduced from the sides of the vacuum chamber to generate the carbenes and enable monolayer formation (Figure 2). After 90 min, the substrate was sonicated in isopropanol for 2 min and rinsed with isopropanol and dichloromethane to remove physisorbed molecules. The functionalized and original substrates were analyzed by XPS and water contact angle goniometry to confirm monolayers formation and calculate molecular coverages. We also conducted a control experiment where the **Si** substrate was exposed to the above deposition conditions but without the UV light.

DOI: 10.1021/acs.langmuir.6b02471
Langmuir XXXX, XXX, XXX−XXX

The long-term stability (up to 14 days of exposure) of the **NHS-diazirine** monolayers on **Si**, **SiN**, and **PUA** was tested at room temperature in air, isopropanol, and water. These conditions were selected as typical environments to which molecular coatings are subjected when stored or chemically modified or in biological applications. The monolayer stability was probed with XPS by monitoring changes in the monolayer and substrate regional signals over time. For each exposure condition, a single chip was used to provide data points for the stability plots to ensure that the observed differences did not originate from the changes in the processing conditions. To reduce errors associated with the drift in the XPS count intensity over time or due to the differences in the sample focus position, the XPS areas of the monolayer signals were normalized with respect to the indigenous substrates signals (Si 2p in **Si** and **SiN** and C 1s in **PUA**). In addition, the stability of the monolayers was confirmed via water contact angle goniometry.

XPS Measurements. XPS spectra were recorded on the Kratos Axis Ultra DLD XPS spectrometer equipped with a mono-Al X-ray source (1468.6 eV). The XPS spectra were collected using the widest lens and largest aperture analyzer settings (~600 × 900 μm substrate area). Multiple sweeps were recorded for the survey and regional scans (typically 7−15 sweeps) to increase signal-to-noise ratio. Unless specified, the electron collection angle Θ in all XPS measurements was zero. The XPS signal areas were measured using Casa XPS software.

Electron Attenuation Length. The values for the attenuated length of F 1s, C 1s, and Si 2p electrons in the monolayer were calculated using NIST Electron Effective-Attenuation-Length Database: F 1s λ = 25.17 Å, C 1s λ = 34.52 Å, and Si 2p λ = 38.62 Å.[51]

Monolayer Thickness. Angle-resolved XPS spectroscopy (ARXPS) was used to measure the thickness of the **NHS-diazirine** films on **Si** and **SiN** and to confirm formation of single monolayers.[52−55] Here, we used eq 1, which describes the relationship between the XPS area intensity of the substrate electrons, the electron collection angle, and the thickness of the film that covers the substrate,

$$I_{B(s)corr} = A(\theta)_{corr} \times I_{B(s)} = I^{inf}_{B(s)} \times \exp\left[-\frac{d}{\lambda_{B(m)} \times \cos(\theta)}\right] \quad (1)$$

where $I_{B(s)corr}$ = corrected area intensity of element B in the substrate; $I_{B(s)}$ = measured area intensity of element B in the substrate; $I^{inf}_{B(s)}$ = bulk area intensity of element B in the unfunctionalized substrate; $A(\theta)$ = correction factor measured on the clean, unfunctionalized substrate; $\lambda_{B(m)}$ = inelastic mean free path (the attenuated length) of electrons B in the monolayer; d = monolayer thickness; and θ = collection angle between the sample normal and the analyzer.

In the ARXPS experiments the regional scans of the background Si 2p signals were recorded at different collection angles and fitted into eq 1 to determine the thickness of the **NHS-diazirine** layer. The XPS spectra were recorded from large analytical areas (~600 × 900 μm) to maintain an adequate signal-to-noise ratio and to limit the exposure of the monolayers to the X-ray radiation. Because of the large analytical area, there was a drop in the signal intensity at the higher collection angles associated with the shallow depth of field of the XPS analyzer. The correction factors for the drop in the Si 2p intensity were measured using clean, unfunctionalized **Si** and **SiN** substrates and then used to adjust the signal intensities of the Si 2p scans from the corresponding substrates modified with the **NHS-diazirine** films (Table 1S: signal intensities, correction factors, and collection angles).

The measured thicknesses (Scheme 1) of the monolayers on **Si** (d = 10.5 Å) and **SiN** (d = 11.1 Å) are in good agreement with the calculated height of a single **NHS-diazirine** molecule (d = 10.75 Å). Considering the relatively rigid nature of the **NHS-diazirine** molecule (two cyclic fragments and high number of sp2 atoms), the height of all **NHS-diazirine** monolayers on different substrates should be similar. Therefore, in all subsequent measurements, we used d = 10.75 Å as the **NHS-diazirine** monolayer thickness on all substrates. We were unable to accurately measure the monolayer thickness on the PUA substrates using ARXPS due to the inability to separate monolayer and background signals in the regional scans of C 1s and N 1s atoms at higher collection angles (both the monolayer and the substrate contain carbon and nitrogen atoms).

Scheme 1. ARXPS Experiments of the NHS-diazirine Monolayers on Si and SiN: Logarithmic Fits of the Corrected Si 2p Signal Areas from the Si and SiN Substrates as a Function of 1/cos(θ), and the Measured Thicknesses of the NHS-diazirine Films

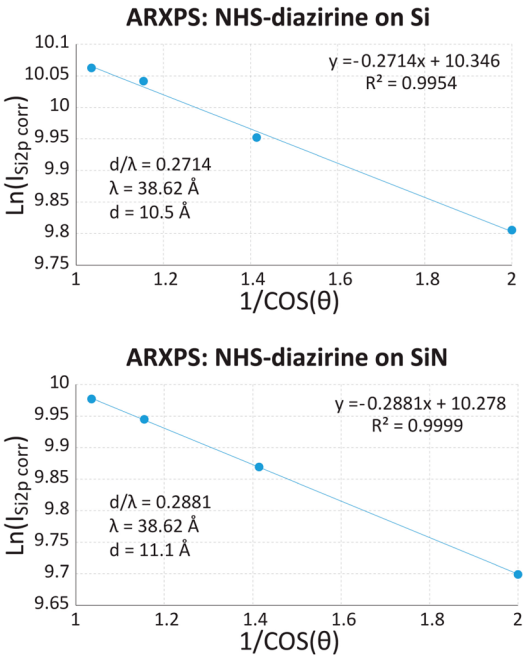

Monolayer Density. Regional, high-resolution C 1s, F 1s, and Si 2p spectra of the functionalized **Si**, **SiN**, and **PUA** were used to calculate the molecular coverage of the chemisorbed carbene molecules (recorded at Θ = 0). We calculated the density of the **NHS-diazirine** films on all three substrates by analyzing distinctive monolayer and substrate XPS signals from each sample.[56−58] This analysis accounts for the influence of the monolayer thickness and density on the intensity of the photoemission from the underlying substrate. In a case of a homogeneous monolayer (m) of thickness d and density ρ_m on the substrate (s), the total XPS intensities $I_{A(m)}$ and $I_{B(s)}$ of the characteristic monolayer (A) and substrate (B) atoms are related to each other through the following equation (eq 2),

$$\frac{I'_{A(m)}}{I'_{B(s)}} = \frac{N_{A(m)}}{N_{B(s)}} \times \frac{1 - \exp(-d/\lambda_{A(m)} \times \cos\theta)}{\exp(-d/\lambda_{B(m)} \times \cos\theta)} \quad (2)$$

$$\frac{I'_{A(m)}}{I'_{B(s)}} = \frac{I_{A(m)} \times \lambda_{B(m)} \times RSF_B}{I_{B(s)} \times \lambda_{A(m)} \times RSF_A}, \frac{N_{A(m)}}{N_{B(s)}} = \frac{\rho_m \times X_{A(m)} \times M_s}{\rho_s \times X_{B(s)} \times M_m}$$

where $I'_{A(m)}$ = correlated area intensity of element A in the monolayer; $I'_{B(s)}$ = correlated area intensity of element B in the substrate; $I_{A(m)}$ = area intensity of element A in the monolayer; $I_{B(s)}$ = area intensity of element B in the substrate; $N_{A(m)}$ = atomic density of element A in the monolayer; $N_{B(s)}$ = atomic density of element B in the substrate; d = monolayer thickness; $\lambda_{A(m)}$ = inelastic mean free path (the attenuated length) of the electrons A in the monolayer; $\lambda_{B(m)}$ = inelastic mean free path (the attenuated length) of the electrons B in the monolayer; θ = the emission angle of the electrons with respect to the surface normal; RSF_A = atomic sensitivity factor of element A; RSF_B = atomic sensitivity factor of element B; ρ_m = monolayer density, ρ_s = substrate density; M_m = monolayer molecular weight; M_s = substrate molecular weight; $X_{A(m)}$ = stoichiometric number of element A in the monolayer; and $X_{B(s)}$ = stoichiometric number of element B in the substrate.

To calculate monolayer densities ρ_m (eq 2), we used peak intensities of F 1s and C(−F)1s atoms as unique monolayer signals $I_{A(m)}$ and Si

DOI: 10.1021/acs.langmuir.6b02471
Langmuir XXXX, XXX, XXX−XXX

2p (**Si** and **SiN**) and C 1s (**PUA**) peak intensities as characteristic substrate signals $I_{B(s)}$. Peak intensities were measured from the regional scans of the corresponding elements using Casa XPS software and atomic relative sensitivity factors of the specific Kratos Ultra DLD XPS instrumentation (Table 2S). We note that the C 1s **PUA** signal consists of photoemissions from both the **PUA** substrate and the **NHS-diazirine** molecule and that these emissions cannot be easily distinguished, except for the characteristic **NHS-diazirine** signal from the fluorine-bound carbon atom C(−F)1s at 293.5 eV (Figure 3). To accurately estimate the intensity of the C 1s photoemission from the **PUA** material, we first calculated the photoemission intensity of the **NHS-diazirine** monolayer from its stoichiometry and the peak area of the C(−F)1s signal and then subtracted the calculated intensity from the overall C 1s XPS intensity of the functionalized **PUA** substrate. In these calculations, we used a predicted density of the **PUA** material (1.5 g/cm^3, calculated using Advanced Chemistry Development (ACD/Laboratories) software, version 11.02) and previously reported densities of 2.33 g/cm^3 for pure polycrystalline Si and 3.4 g/cm^3 for silicon nitride.[59] The stoichiometries of the **NHS-diazirine** monolayer and **PUA** were calculated from their chemical formulas. The stoichiometry of the clean **SiN** film was measured by XPS.

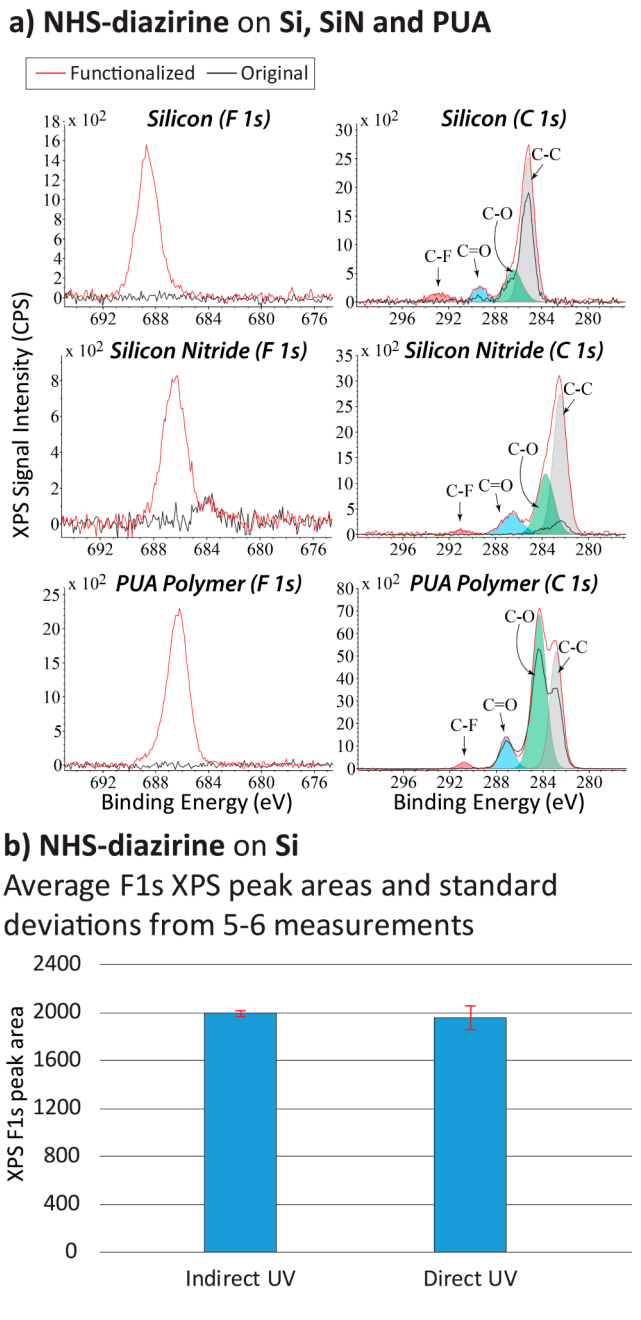

Figure 3. (a) F 1s (left column) and C 1s (right column) XPS spectra of the original (black) and functionalized (red) **Si**, **SiN**, and **PUA** substrates. C 1s XPS spectra of the functionalized substrates show peak components that correspond to carbon atoms of different hybridization and bonding. (b) Average F 1s XPS peak areas and standard deviations (5−6 measurements) of the **NHS-diazirine** monolayers on **Si** in the areas that were directly illuminated with the UV light and shielded from the direct UV illumination.

RESULTS AND DISCUSSION

Vapor-Phase Carbenylation. The surface attachment of the carbene species generated from the **NHS-diazirine** molecules was confirmed by XPS and water contact angle goniometry. Figure 3a shows regional F 1s and C 1s XPS spectra of the **Si**, **SiN**, and **PUA** substrates before (black) and after (red) the reaction with the carbene molecules. F 1s and C 1s XPS spectra confirm the attachment of the carbene molecule on all three substrates. The functionalized substrates show prominent fluorine peak from the CF_3- group of the **NHS-diazirine** at 688 eV (**Si**) and 686.5 eV (**SiN** and **PUA**). In contrast, the original **Si** and **PUA** substrates lack F 1s signals, whereas **SiN** contains a small F 1s peak at 683.5 eV, which is associated with the buffered oxide etch (BOE: NH_4F) step. The XPS spectrum of the control **Si** substrate, which was exposed to the same deposition conditions but without the UV light, does not contain the F 1s signal. C 1s XPS spectra of the functionalized **Si** and **SiN** show a general increase in the carbon intensity from the unmodified **Si** and **SiN** that contain typical C 1s peaks from nonspecifically adsorbed organic molecules. The functionalized **Si** and **SiN** samples also contain additional C(=O)1s and C(−F)1s peaks at 288−291.5 eV and 293.5.5−295 eV that correspond to the C=O and C−F bonds in the **NHS-diazirine** molecule. The C 1s spectrum of the functionalized **PUA** is similar to that of the unmodified **PUA** substrate, with the exception of an additional C(−F)1s peak at 293 eV from the C−F C 1s electrons. The atomic concentration ratio of the fluorine atoms to the fluorine-bound carbon atoms in all three monolayers confirms the presence of an intact CF_3 group (**Si**: 2.9:1; **SiN**: 2.8:1; **PUA**: 3.3:1) and serves as additional evidence of the **NHS-diazirine** attachment.

We examined the uniformity of the **NHS-diazirine** films on **Si** and the dependence of the molecular coverage on the substrate and UV source positions. In these experiments, we reacted two silicon chips (2 × 2 cm^2) with **NHS-diazirine** molecules and measured the XPS F 1s peak areas in 5−6 different locations on each substrate (Figure 3b and Table3S). One of the substrates was positioned under the diazirine source and was directly irradiated with the UV light (e.g., line-of-sight evaporation, **Direct UV** on Figure 3b), and the second substrate was located further away from the source in a nonline-of-sight position from both the source and the UV light (**Indirect UV** on Figure 3b). The analyzed locations on each substrate were randomly selected to cover the entire substrate area. Figure 3b shows normalized average F 1s XPS peak areas and their standard deviations of the **Indirect UV** and **Direct UV** substrates. These measurements show that the vapor-phase carbene reactions produce uniform films, whose coverage has no significant dependence on the substrate position in relation to the carbene and UV light sources. The fact that the chemisorbed diazirine films were formed on the substrate whose surface was not directly exposed to the UV light

DOI: 10.1021/acs.langmuir.6b02471
Langmuir XXXX, XXX, XXX−XXX

indicates that the carbene formation happens in the vapor phase and that the generated carbenes have adequate life times to establish a uniform vapor pressure inside the deposition chamber. These experiments suggest that the vapor-phase carbenylation can be used in the functionalization of nanostructured and porous materials with uniform molecular coatings. The coverage of the **NHS-diazirine** molecules was slightly lower (by 1.3%) and less uniform ($\sigma_{(\text{indirect})}$ = 1.1% versus $\sigma_{(\text{direct})}$ = 4.9%) on the substrate that was directly positioned under the carbene source. This can be explained by a faster physisorption rate of the carbene or **NHS-diazirine** molecules on the substrate positioned in the line-of-sight with the source. Rapid physisorption can cover the active surface sites with the unreacted molecules, reducing the total coverage of the chemisorbed species.

Monolayer Surface Coverage. Table 1 shows densities of the **NHS-diazirine** monolayers on **Si**, **SiN**, and **PUA** calculated

Table 1. (Top) Measured Densities and Contact Angles of the NHS-diazirine Monolayers on Si, SiN, and PUA; (Bottom) Comparison of the XPS Measured Monolayer Densities and Water Contact Angles of the NHS-diazirine Monolayers on Si, SiN, and PUA

Substrate	Monolayer density (g/cm^3)	
	From F1s	From C(-F)1s
Si	1.67	1.67
SiN	1.59	1.60
PUA	1.48	1.26
Substrate	**Monolayer surface coverage (moles/cm^2; molecules/nm^2)**	
	From F1s	From C(-F)1s
Si	5.98×10^{-10} 3.60	5.98×10^{-10} 3.60
SiN	5.70×10^{-10} 3.43	5.73×10^{-10} 3.45
PUA	5.30×10^{-10} 3.19	4.52×10^{-10} 2.72
Substrate	**Contact angle (water): static, advancing, receding**	
	Substrate	Monolayer
Si	38.2°, 47.3°, 24.6°	85.0°, 85.4°, 30.2°
SiN	36.1°, 48.0°, 21.6°	80.4°, 83.2°, 31.1°
PUA	59.9°, 68.4°, 25°	76.4°, 79.2°, 32°

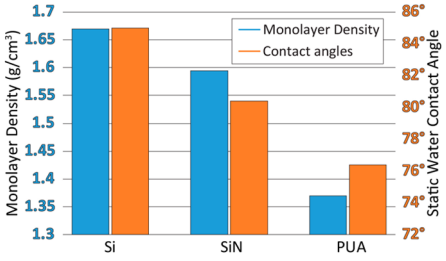

using eq 1 from the measured intensities of the F 1s or C(−F)1s (monolayer) and Si 2p or C 1s (substrate) XPS signals. Comparison of the monolayer densities calculated from the F 1s and C(−F)1s signals shows that they are in good agreement with each other, validating our assumptions about the monolayer structure and composition, as well as the density and stoichiometry of the underlying substrates.

The measured surface densities of the **NHS-diazirine** monolayers on **Si** (1.67 g/cm^3) and **SiN** (1.60 g/cm^3) are in good agreement with each other and with the predicted density of the solid molecule (1.68 g/cm^3). These measurements suggest that **NHS-diazirine** monolayers on **Si** and **SiN** achieve almost complete surface coverage and packing density similar to the bulk solid phase. Calculated mass densities of 1.67 and 1.60 g/cm^3 translate to 6.0×10^{-10} and 5.7×10^{-10} mol/cm^2 (or 3.6 and 3.4 molecules/nm^2) molecular surface densities for a 10.75 Å thick monolayer with M_W = 300 g/mol. The measured molecular coverage of the **NHS-diazirine** monolayers on **Si** and **SiN** is approximately two times lower than the reported molecular coverage of the highly ordered SAMs of aliphatic thiols on gold ($\sim9\times10^{-10}$ mol/cm^2).[60] High mass density and low molecular coverage suggest that the **NHS-diazirine** monolayers on **Si** and **SiN** are closely packed but lack an ordered arrangement of typical SAMs

The measured density of the **NHS-diazirine** monolayer on **PUA** (~1.4 g/cm^3) is lower by ~15% than its density on **Si** and **SiN**. This result is expected, considering that **Si** and **SiN** have higher surface coverage of the carbene-reactive Si−H bonds than the density of the C−H groups on **PUA**.

Differences in the water contact angles between the pure substrates and the monolayers further confirm successful modification of all three materials with **NHS-diazirine**. Monolayers on all substrates demonstrate slightly hydrophobic static water contact angles, which is consistent with the **NHS-diazirine** structure that contains a hydrophobic CF_3 group and a polar NHS moiety. Notably, a slight decrease in the monolayer water contact angle in the **Si−SiN−PUA** sequence correlates with the decrease in the monolayer density in the same **Si−SiN−PUA** order (Table 1). Large hysteresis between advancing and receding monolayer contact angles indicates that these monolayers lack symmetrical order.

The provided analysis of the XPS data and water contact angle measurements suggests that the described vapor-phase carbenylation offers a convenient way to modify a variety of substrates with functional monolayers of organic molecules using a unified set of experimental condition. Our measurements indicate that the carbenylation reaction yields well-packed monolayers, whose density depends on the surface concentration of the carbene-reactive groups, approaching bulk solid density values on the interfaces with high surface coverage of the Si−H species. This strategy offers a significant advantage over similar solution-phase processing in terms of the variety of materials, topographical surface structures, and overall substrate dimensions that can be processed by the vapor-phase deposition. Solution-phase carbene reactions impose very strict requirements on the chemical inertness of the solvent, limiting traditional choices to carbon tetrachloride and cyclohexane. Many polymers and thin organic films swell, degrade, or simply dissolve in these solvents, making their functionalization with diazirine solutions impossible. UV-catalyzed solution processing of inorganic materials is also complicated by low solubility of diazirines and fast solvent-evaporation rates. Nanostructured, rough, and porous materials (colloids, membranes, catalyst supports, or patterned interfaces) can also benefit from the vapor-based deposition, which avoids undesired capillary effects and material concentration and crystallization during drying. Vacuum-phase processing also makes the method compatible with the traditional physical vapor deposition (PVD) equipment, potentially permitting the manufacturing of hybrid monolayer-thin film devices in a single apparatus.

Monolayer Stability. The stability of the **NHS-diazirine** monolayers on **Si**, **SiN**, and **PUA** was measured in air, isopropanol, and water and was plotted as a percent change of the initial XPS peak area (at t = 0 h) over time (Figures 4 and 4S). We expected that the substrate reactivity, specifically its tendency toward oxidation, will have an effect on the stability of the **NHS-diazirine** monolayers. Traditional, well-packed SAMs

DOI: 10.1021/acs.langmuir.6b02471
Langmuir XXXX, XXX, XXX−XXX

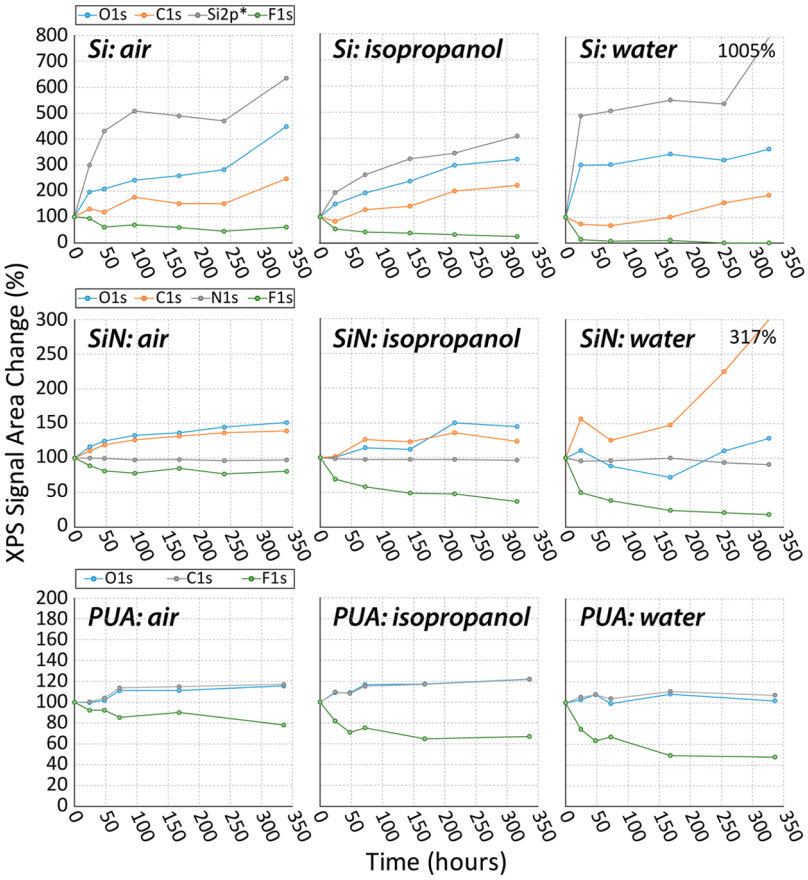

Figure 4. Stability measurements of the **NHS-diazirine** monolayers on **Si**, **SiN**, and **PUA** substrates exposed to air, isopropanol and water. Plots show changes (%) in the normalized XPS signal areas of the **NHS-diazirine** monolayers on **Si**, **SiN**, and **PUA** as functions of time and environment; *peak area of the Si 2p electrons bonded to oxygen atoms.

can form effective diffusion barriers on chemically active interfaces, thus limiting their degradation in reactive conditions. We showed in the previous section that the molecular surface coverage of the **NHS-diazirine** monolayers is lower than that of the traditional, highly organized SAMs. Thus, we assumed that they cannot serve as efficient barriers to oxygen and water molecules on top of the oxidation-prone H−Si and H−SiN substrates. However, considering that the **NHS-diazirine** monolayers are attached to the substrates via thermodynamically and kinetically stable Si−C and C−C bonds, we also expected that they will show good stability on the chemically inert interfaces and in the environments that do not promote rapid oxidation.

The stability measurements of the **NHS-diazirine** monolayers (Figure 4) largely confirm our assumptions. Hydrogen-terminated H−Si typically forms a thin native oxide layer within 10 min when exposed to air and even more rapidly in water. Stability plots (Figure 4, top) of the **NHS-diazirine** monolayer on **Si** show that in all environments silicon substrates undergo oxidation, which is evident from the substantial increase over time in the XPS oxygen (O 1s peak at 529 eV) and silicon oxide peak areas (Si 2p peak at 99.4 eV). The plots also show the increase in the carbon concentration over time, which is likely due to the accumulation of nonspecifically adsorbed organic molecules. At the same time, after 300 h of exposure the fluorine concentration (F 1s peak at 688 eV), which correlates with the concentration of the monolayer molecules, dropped by 39% in air, 75% in isopropanol, and 100% in water. These measurements demonstrate that the **NHS-diazirine** monolayers on **Si** show adequate stability in air (oxidative, but not hydrolytic environment) even after 350 h of exposure but degrade rapidly within 24 h when exposed to both hydrolytic and oxidative conditions (water). Isopropanol, which has reduced hydrolytic activity compared to water, promotes partial desorption of the **NHS-diazirine** monolayers. We note that the decrease in the F 1s XPS signal intensity can partially be attributed to the accumulation of physisorbed materials on top of the substrates, which reduces the inelastic mean free path of the photoelectrons emitted from the monolayer atoms (Figure 4, C 1s signal changes).

We compared the stability of the **NHS-diazirine** monolayers on H−Si with the stability of the perfluorinated (1*H*,1*H*,2*H*,2*H*-tridecafluorooct-1-yl)phosphonic acid (**F-PA**) monolayers on oxidized Si. **F-PA** forms dense, well-packed SAMs on oxides that are known for their excellent thermal stability and are often used in electronic devices to control work functions of the transparent oxide and metal−oxide electrodes.[61−65] Figure 5S shows that the **F-PA** SAMs on the plasma-oxidized silicon have good long-term stability in air (F 1s XPS signal drops by 40% after 170 h of exposure) but rapidly degrade in water due to the hydrolytic nature of the Si−O−P bonds (F 1s XPS signal drops by 82% after 24 h and disappear completely after 170 h of exposure). At the same time, the underlying Si/SiO_2 substrate show relatively small changes in its composition (O 1s signals).

NHS-diazirine monolayers on **SiN** show improved stability over the similar monolayers on **Si**: the F 1s signal of the monolayers on **SiN** dropped by 19% in air, 63% in isopropanol,

DOI: 10.1021/acs.langmuir.6b02471
Langmuir XXXX, XXX, XXX−XXX

and 82% in water after 300 h of exposure. We observed a large increase in the nonspecifically adsorbed organic material on the **SiN NHS-diazirine** monolayers after the exposure to water. The overall C 1s XPS signal area of the carbon in this monolayer increased by more than 200%. The accumulation of the organic material on top of the monolayer partially contributes to the observed decrease of the F 1s signal area. The improved stability of the monolayers on **SiN** is likely attributed to a slower oxidation rate of the H−SiN compared to H−Si. This assumption is supported by the measurements of the oxygen content in **SiN** and **Si** monolayers over time. In all environments, the O 1s signal area increased by ∼300−400% on **Si** and only by ∼25−50% on **SiN** (Figure 4).

PUA is a glassy polymer that is often used in microcontact printing as a stamp material due to its high chemical inertness and good mechanical stability. It can withstand exposure to various organic chemicals and does not degrade at high temperatures.[66,67] However, it swells if soaked in halogenated organic solvents, which promotes its mechanical degradation. Therefore, it cannot be functionalized using liquid-phase carbene reactions. In contrast, vapor-phase carbenylation provides a convenient way to modify **PUA** surface with functional monolayers. As expected, **NHS-diazirine** monolayers on chemically inert **PUA** show good stability when exposed to air, isopropanol, and water, even despite their lower density and surface coverage. The overall drop in the **PUA** monolayer F 1s signal after 340 h of exposure was 21% in air, 33% in isopropanol, and 53% in water (Figure 4).

In addition to the XPS measurements, the hydrolytic stability of the monolayers exposed to water was assessed by the contact angle measurements. Figure 6S shows water contact angles of the monolayers on **Si**, **SiN**, and **PUA** after exposure to water for up to 14 days. Monolayers on **Si** show rapid decrease in the water contact angles after exposure to water for 24 h, whereas monolayers on **PUA** demonstrate no significant changes in the water contact angles even after 14 days of exposure. Monolayers on **SiN** demonstrate intermediate stability in water, which is likely associated with the slower oxidation rate of passivated silicon nitride. These measurements are in a good agreement with the XPS measurements.

Our combined XPS and water contact angle measurements suggest that even though the **NHS-diazirine** monolayers are not stabilized by the extensive intermolecular interactions, they can still act as a viable alternative to the traditional SAMs, especially in the environments that do not promote rapid substrate reactions or on chemically inert interfaces.

CONCLUSIONS

Our work shows that the presented carbenylation strategy can be used to form dense monolayers of functional organic molecules on passivated hard (silicon and silicon nitride) and soft (urethane−acrylate polymer) interfaces. These monolayers are attached to the surfaces via nonhydrolytic Si−C and C−C bonds, making them less prone to hydrolytic cleavage than typical SAMs on oxides and metals. However, due to the nonsymmetrical structure of **NHS-diazirine**, its monolayers have lower molecular surface coverage than the traditional aliphatic SAMs and lack the ability to act as efficient diffusion barriers against substrate degradation. By examining monolayers on substrates with different oxidation propensities, we demonstrated that the stability of the **NHS-diazirine** monolayers is primarily determined by the reactivity of the underlying substrates and not by the monolayer attachment chemistry. Therefore, the described functionalization method can serve as a complementary technique to the traditional SAM methodology in applying functional monomolecular coatings on substrates that are typically incompatible with the traditional molecular self-assembly (e.g., organic interfaces or chemically inert inorganics). Functionalization of polymers and organic thin films with monomolecular coatings can enable a myriad of applications in which such material properties as adhesion, friction, chemical specificity, or electron/hole injection barriers are controlled with a single functional monolayer, without modifying the bulk. Our future work will investigate some of the mentioned utilities of the carbenylated monolayers.

ASSOCIATED CONTENT

Supporting Information

The Supporting Information is available free of charge on the ACS Publications website at DOI: 10.1021/acs.langmuir.6b02471.

Experimental details, characterization methods, and additional data on the monolayer density and stability measurements (PDF)

AUTHOR INFORMATION

Corresponding Author

*E-mail: alexander.shestopalov@rochester.edu.

Notes

The authors declare no competing financial interest.

ACKNOWLEDGMENTS

Financial support of NSF (DMR 1228889) is gratefully acknowledged

REFERENCES

(1) Schoenbaum, C. A.; Schwartz, D. K.; Medlin, J. W. Controlling the Surface Environment of Heterogeneous Catalysts Using Self-Assembled Monolayers. *Acc. Chem. Res.* **2014**, *47* (4), 1438−1445.

(2) Turchanin, A.; Gölzhäuser, A. Carbon Nanomembranes From Self-Assembled Monolayers: Functional Surfaces Without Bulk. *Prog. Surf. Sci.* **2012**, *87* (5−8), 108−162.

(3) Kwok, C. S.; Mourad, P. D.; Crum, L. A.; Ratner, B. D. Surface Modification of Polymers with Self-Assembled Molecular Structures: Multitechnique Surface Characterization†. *Biomacromolecules* **2000**, *1* (1), 139−148.

(4) Gholamrezaie, F.; Mathijssen, S. G. J.; Smits, E. C. P.; Geuns, T. C. T.; van Hal, P. A.; Ponomarenko, S. A.; Flesch, H.-G.; Resel, R.; Cantatore, E.; Blom, P. W. M.; de Leeuw, D. M. Ordered Semiconducting Self-Assembled Monolayers on Polymeric Surfaces Utilized in Organic Integrated Circuits. *Nano Lett.* **2010**, *10* (6), 1998−2002.

(5) Penner, P.; Zhang, X.; Marschewski, E.; Behler, F.; Angelova, P.; Beyer, A.; Christoffers, J.; Gölzhäuser, A. Charge Transport through Carbon Nanomembranes. *J. Phys. Chem. C* **2014**, *118* (37), 21687−21694.

(6) Angel, F. A.; Lyubarskaya, Y. L.; Shestopalov, A. A.; Tang, C. W. Degradation of Self-Assembled Monolayers in Organic Photovoltaic Devices. *Org. Electron.* **2014**, *15* (12), 3624−3631.

(7) Bowers, C. M.; Zhang, M.; Lyubarskaya, Y. L.; Toone, E. J.; Tang, C.; Shestopalov, A. A. Structural Modifications in Bilayered Molecular Systems Lead to Predictable Changes in Their Electronic Properties. *Adv. Mater. Interfaces* **2014**, *1* (2), 1300109.

(8) Nuzzo, R. G.; Allara, D. L. Adsorption of Bifunctional Organic Disulfides on Gold Surfaces. *J. Am. Chem. Soc.* **1983**, *105* (13), 4481−4483.

(9) Ulman, A. Formation and Structure of Self-Assembled Monolayers. *Chem. Rev.* **1996**, *96* (4), 1533−1554.

DOI: 10.1021/acs.langmuir.6b02471
Langmuir XXXX, XXX, XXX−XXX

(10) Haensch, C.; Hoeppener, S.; Schubert, U. S. Chemical Modification of Self-assembled Silane Based Monolayers by Surface Reactions. *Chem. Soc. Rev.* **2010**, *39* (6), 2323−2334.
(11) Love, J. C.; Estroff, L. A.; Kriebel, J. K.; Nuzzo, R. G.; Whitesides, G. M. Self-Assembled Monolayers of Thiolates on Metals as a Form of Nanotechnology. *Chem. Rev.* **2005**, *105* (4), 1103−1169.
(12) Penfold, J.; Thomas, R. K. Probing Surfactant Adsorption at the Solid−Solution Interface by Neutron Reflectometry. In *Interface Science and Technology*; Toyoko, I., Ed.; Elsevier: 2007; Vol. *14*, pp 87−115.
(13) O'Dwyer, C.; Gay, G.; Viaris de Lesegno, B.; Weiner, J. The Nature of Alkanethiol Self-Assembled Monolayer Adsorption on Sputtered Gold Substrates. *Langmuir* **2004**, *20* (19), 8172−8182.
(14) Sun, L.; Crooks, R. M. Indirect Visualization of Defect Structures Contained Within Self-Assembled Organomercaptan Monolayers: Combined Use of Electrochemistry and Scanning Tunneling Microscopy. *Langmuir* **1993**, *9* (8), 1951−1954.
(15) Poirier, G. E. Mechanism of Formation of Au Vacancy Islands in Alkanethiol Monolayers on Au(111). *Langmuir* **1997**, *13* (7), 2019−2026.
(16) Poirier, G. E. Characterization of Organosulfur Molecular Monolayers on Au(111) using Scanning Tunneling Microscopy. *Chem. Rev.* **1997**, *97* (4), 1117−1128.
(17) Claridge, S. A.; Liao, W.-S.; Thomas, J. C.; Zhao, Y.; Cao, H. H.; Cheunkar, S.; Serino, A. C.; Andrews, A. M.; Weiss, P. S. From the Bottom up: Dimensional Control and Characterization in Molecular Monolayers. *Chem. Soc. Rev.* **2013**, *42* (7), 2725−2745.
(18) Li, X.-M.; Huskens, J.; Reinhoudt, D. N. Reactive Self-Assembled Monolayers on Flat and Nanoparticle Surfaces, and Their Application in Soft and Scanning Probe Lithographic Nanofabrication Technologies. *J. Mater. Chem.* **2004**, *14* (20), 2954−2971.
(19) Smith, R. K.; Lewis, P. A.; Weiss, P. S. Patterning Self-assembled Monolayers. *Prog. Surf. Sci.* **2004**, *75* (1−2), 1−68.
(20) Sullivan, T. P.; Huck, W. T. S. Reactions on Monolayers: Organic Synthesis in Two Dimensions. *Eur. J. Org. Chem.* **2003**, *2003* (1), 17−29.
(21) Tamada, K.; Hara, M.; Sasabe, H.; Knoll, W. Surface Phase Behavior of n-Alkanethiol Self-Assembled Monolayers Adsorbed on Au(111): An Atomic Force Microscope Study. *Langmuir* **1997**, *13* (6), 1558−1566.
(22) Stranick, S. J.; Atre, S. V.; Parikh, A. N.; Wood, M. C.; Allara, D. L.; Winograd, N.; Weiss, P. S. Nanometer-scale Phase Separation in Mixed Composition Self-Assembled Monolayers. *Nanotechnology* **1996**, *7* (4), 438.
(23) Folkers, J. P.; Laibinis, P. E.; Whitesides, G. M. Self-Assembled Monolayers of Alkanethiols on Gold: Comparisons of Monolayers Containing Mixtures of Short- and Long-Chain Constituents with Methyl and Hydroxymethyl Terminal Groups. *Langmuir* **1992**, *8* (5), 1330−41.
(24) Colavita, P. E.; Sun, B.; Tse, K.-Y.; Hamers, R. J. Photochemical Grafting of n-Alkenes onto Carbon Surfaces: the Role of Photoelectron Ejection. *J. Am. Chem. Soc.* **2007**, *129* (44), 13554−13565.
(25) Leroux, Y. R.; Fei, H.; Noël, J.-M.; Roux, C.; Hapiot, P. Efficient Covalent Modification of a Carbon Surface: Use of a Silyl Protecting Group To Form an Active Monolayer. *J. Am. Chem. Soc.* **2010**, *132* (40), 14039−14041.
(26) Yang, W.; Auciello, O.; Butler, J. E.; Cai, W.; Carlisle, J. A.; Gerbi, J. E.; Gruen, D. M.; Knickerbocker, T.; Lasseter, T. L.; Russell, J. N.; Smith, L. M.; Hamers, R. J. DNA-Modified Nanocrystalline Diamond Thin-Films as Stable, Biologically Active Substrates. *Nat. Mater.* **2002**, *1* (4), 253−257.
(27) Stavis, C.; Clare, T. L.; Butler, J. E.; Radadia, A. D.; Carr, R.; Zeng, H.; King, W. P.; Carlisle, J. A.; Aksimentiev, A.; Bashir, R.; Hamers, R. J. Surface Functionalization of Thin-Film Diamond for Highly Ttable and Selective Biological Interfaces. *Proc. Natl. Acad. Sci. U. S. A.* **2011**, *108* (3), 983−988.
(28) Buriak, J. M. Organometallic Chemistry on Silicon Surfaces: Formation of Functional Monolayers Bound Through Si-C Bonds. *Chem. Commun.* **1999**, No. 12, 1051−1060.
(29) Puniredd, S. R.; Assad, O.; Haick, H. Highly Stable Organic Monolayers for Reacting Silicon with Further Functionalities: The Effect of the C-C Bond nearest the Silicon Surface. *J. Am. Chem. Soc.* **2008**, *130* (41), 13727−13734.
(30) Assad, O.; Puniredd, S. R.; Stelzner, T.; Christiansen, S.; Haick, H. Stable Scaffolds for Reacting Si Nanowires with Further Organic Functionalities while Preserving Si-C Passivation of Surface Sites. *J. Am. Chem. Soc.* **2008**, *130* (52), 17670−17671.
(31) Wei, S.; Wang, J.; Guo, D.-J.; Chen, Y.-Q.; Xiao, S.-J. Grafting Organic and Biomolecules on H-terminated Porous Silicon from a Diazirine. *Chem. Lett.* **2006**, *35* (10), 1172−1173.
(32) Bowers, C. M.; Shestopalov, A. A.; Clark, R. L.; Toone, E. J. Multicomponent Patterning of Indium Tin Oxide. *ACS Appl. Mater. Interfaces* **2012**, *4* (8), 3932−3937.
(33) Bowers, C. M.; Toone, E. J.; Clark, R. L.; Shestopalov, A. A. Soft Lithographic Functionalization and Patterning Oxide-free Silicon and Germanium. *J. Visualized Exp.* **2011**, *58*, e3478.
(34) Morris, C. J.; Shestopalov, A. A.; Gold, B. H.; Clark, R. L.; Toone, E. J. Patterning NHS-Terminated SAMs on Germanium. *Langmuir* **2011**, *27* (10), 6486−6489.
(35) Shestopalov, A. A.; Morris, C. J.; Vogen, B. N.; Hoertz, A.; Clark, R. L.; Toone, E. J. Soft-Lithographic Approach to Functionalization and Nanopatterning Oxide-Free Silicon. *Langmuir* **2011**, *27* (10), 6478−6485.
(36) Bond, M. R.; Zhang, H.; Kim, J.; Yu, S.-H.; Yang, F.; Patrie, S. M.; Kohler, J. J. Metabolism of Diazirine-Modified N-Acetylmannosamine Analogues to Photo-Cross-Linking Sialosides. *Bioconjugate Chem.* **2011**, *22* (9), 1811−1823.
(37) Choi, J.; Wang, N. S.; Reipa, V. Conjugation of the Photoluminescent Silicon Nanoparticles to Streptavidin. *Bioconjugate Chem.* **2008**, *19* (3), 680−685.
(38) Gomes, A. F.; Gozzo, F. C. Chemical Cross-Linking with a Diazirine Photoactivatable Cross-Linker Investigated by MALDI- and ESI-MS/MS. *J. Mass Spectrom.* **2010**, *45* (8), 892−899.
(39) McCormick, A. M.; Wijekoon, A.; Leipzig, N. D. Specific Immobilization of Biotinylated Fusion Proteins NGF and Sema3A Utilizing a Photo-Cross-Linkable Diazirine Compound for Controlling Neurite Extension. *Bioconjugate Chem.* **2013**, *24* (9), 1515−26.
(40) Tomohiro, T.; Hatanaka, Y. Novel Fluorophore Tagging of Protein at the Interacting Site by Photocross-Linking. *Photomed. Photobiol.* **2011**, *33*, 1−2.
(41) Tomohiro, T.; Kato, K.; Masuda, S.; Kishi, H.; Hatanaka, Y. Photochemical Construction of Coumarin Fluorophore on Affinity-Anchored Protein. *Bioconjugate Chem.* **2011**, *22* (3), 315−318.
(42) Vila-Perello, M.; Pratt, M. R.; Tulin, F.; Muir, T. W. Covalent Capture of Phospho-Dependent Protein Oligomerization by Site-Specific Incorporation of a Diazirine Photo-Cross-Linker. *J. Am. Chem. Soc.* **2007**, *129* (26), 8068−8069.
(43) Kambe, T.; Correia, B. E.; Niphakis, M. J.; Cravatt, B. F. Mapping the Protein Interaction Landscape for Fully Functionalized Small-Molecule Probes in Human Cells. *J. Am. Chem. Soc.* **2014**, *136* (30), 10777−10782.
(44) Kawaguchi, Y.; Kuwata, K.; Tanaka, G.; Takeuchi, T.; Nakase, I.; Futaki, S. Identifying Proteins Responsible to the Cellular Uptake of Octaarginine Using Photo-Crosslinking. *Pept. Sci.* **2013**, *50*, 361−362.
(45) Li, Z.; Wang, D.; Li, L.; Pan, S.; Na, Z.; Tan, C. Y. J.; Yao, S. Q. "Minimalist" Cyclopropene-Containing Photo-Cross-Linkers Suitable for Live-Cell Imaging and Affinity-Based Protein Labeling. *J. Am. Chem. Soc.* **2014**, *136* (28), 9990−9998.
(46) Lin, E.-W.; Boehnke, N.; Maynard, H. D. Protein-Polymer Conjugation via Ligand Affinity and Photoactivation of Glutathione S-Transferase. *Bioconjugate Chem.* **2014**, *25* (10), 1902−1909.
(47) Naik, R.; Won, M.; Ban, H. S.; Bhattarai, D.; Xu, X.; Hong, Y. S.; Eo, Y.; Singh, S.; Choi, Y.; Ahn, H.-C.; Lee, K. Synthesis and Structure-Activity Relationship Study of Chemical Probes as Hypoxia Induced Factor-1α/Malate Dehydrogenase 2 Inhibitor. *J. Med. Chem.* **2014**, *57*, 9522.
(48) Zhang, H.; Song, Y.; Zou, Y.; Ge, Y.; An, Y.; Ma, Y.; Zhu, Z.; Yang, C. J. A Diazirine-Based Photoaffinity Probe for Facile and

DOI: 10.1021/acs.langmuir.6b02471
Langmuir XXXX, XXX, XXX−XXX

Efficient Aptamer-Protein Covalent Conjugation. *Chem. Commun. (Cambridge, U. K.)* **2014**, *50* (38), 4891−4894.
(49) Hatanaka, Y.; Nakamura, N.; Wakabayashi, M.; Fujioka, T.; Kikuchi, T. Synthesis and Characterization of Novel Photoreactive Naltrexone Analogs as Isomeric Carbene-Generating Probes for Opioid Receptors. *Heterocycles* **1996**, *43* (3), 519−22.
(50) Nassal, M. 4-(1-Azi-2,2,2-trifluoroethyl)benzoic Acid, a Highly Photolabile Carbene Generating Label Readily Fixable to Biochemical Agents. *Liebigs Annalen der Chemie* **1983**, *1983* (9), 1510−23.
(51) Powell, C. J.; Jablonski, A. *NIST Electron Effective-Attenuation-Length Database*, version 1.3; National Institute of Standards and Technology: Gaithersburg, MD, 2011.
(52) Briggs, D.; Seah, M. P. *Practical Surface Analysis, Auger and X-ray Photoelectron Spectroscopy*; Wiley: 1990.
(53) Shircliff, R. A.; Stradins, P.; Moutinho, H.; Fennell, J.; Ghirardi, M. L.; Cowley, S. W.; Branz, H. M.; Martin, I. T. Angle-Resolved XPS Analysis and Characterization of Monolayer and Multilayer Silane Films for DNA Coupling to Silica. *Langmuir* **2013**, *29* (12), 4057−4067.
(54) Lockett, V.; Sedev, R.; Bassell, C.; Ralston, J. Angle-resolved X-ray photoelectron spectroscopy of the surface of imidazolium ionic liquids. *Phys. Chem. Chem. Phys.* **2008**, *10* (9), 1330−1335.
(55) Laibinis, P. E.; Bain, C. D.; Whitesides, G. M. Attenuation of photoelectrons in monolayers of n-alkanethiols adsorbed on copper, silver, and gold. *J. Phys. Chem.* **1991**, *95* (18), 7017−7021.
(56) Seah, M. P. Quantification of AES and XPS. In *Practical Surface Analysis by Auger and X-ray Photoelectron Spectroscopy*; Briggs, D., Seah, M. P., Eds.; John Wiley and Sons: 1983; Vol. *1*, p 211.
(57) Seah, M. P.; Spencer, S. J. Ultrathin SiO2 on Si. II. Issues in Quantification of the Oxide Thickness. *Surf. Interface Anal.* **2002**, *33* (8), 640−652.
(58) Hesse, R.; Streubel, P.; Szargan, R. Improved Accuracy of Quantitative XPS Analysis Using Predetermined Spectrometer Transmission Functions with UNIFIT 2004. *Surf. Interface Anal.* **2005**, *37* (7), 589−607.
(59) Taft, E. A. Characterization of Silicon Nitride Films. *J. Electrochem. Soc.* **1971**, *118* (8), 1341−1346.
(60) Suroviec, A. H. Determining Surface Coverage of Self-Assembled Monolayers on Gold Electrodes. *Chem. Educ.* **2012**, *17*, 83−85.
(61) Saio, T.; Kumon, S.; Saito, M.; Arata, S.; Nanai, H.; Akamatsu, Y. Liquid Chemical for Forming Protecting Film on Textured Substrate. US20120174945A1, 2012.
(62) Gliboff, M.; Li, H.; Knesting, K. M.; Giordano, A. J.; Nordlund, D.; Seidler, G. T.; Bredas, J.-L.; Marder, S. R.; Ginger, D. S. Competing Effects of Fluorination on the Orientation of Aromatic and Aliphatic Phosphonic Acid Monolayers on Indium Tin Oxide. *J. Phys. Chem. C* **2013**, *117* (29), 15139−15147.
(63) Ishizaki, T.; Okido, M.; Masuda, Y.; Saito, N.; Sakamoto, M. Corrosion Resistant Performances of Alkanoic and Phosphonic Acids Derived Self-Assembled Monolayers on Magnesium Alloy AZ31 by Vapor-Phase Method. *Langmuir* **2011**, *27* (10), 6009−6017.
(64) Wang, H.; Gomez, E. D.; Guan, Z.; Jaye, C.; Toney, M. F.; Fischer, D. A.; Kahn, A.; Loo, Y.-L. Tuning Contact Recombination and Open-Circuit Voltage in Polymer Solar Cells via Self-Assembled Monolayer Adsorption at the Organic-Metal Oxide Interface. *J. Phys. Chem. C* **2013**, *117* (40), 20474−20484.
(65) Wang, M.; Hill, I. G. Fluorinated Alkyl Phosphonic Acid SAMs Replace PEDOT:PSS in Polymer Semiconductor Devices. *Org. Electron.* **2012**, *13* (3), 498−505.
(66) Li, J.; Xu, L.; Kim, S.; Shestopalov, A. A. Urethane-Acrylate Polymers in High-Resolution Contact Printing. *J. Mater. Chem. C* **2016**, *4* (19), 4155−4165.
(67) Li, J.; Xu, L.; Tang, C. W.; Shestopalov, A. A. High-Resolution Organic Light-Emitting Diodes Patterned via Contact Printing. *ACS Appl. Mater. Interfaces* **2016**, *8*, 16809−16815.

DOI: 10.1021/acs.langmuir.6b02471
Langmuir XXXX, XXX, XXX−XXX